

Craig A. Steeves

Research Associate
Department of Mechanical and Aerospace
Engineering,
Princeton University,
Engineering Quad,
Olden Street,
Princeton, NJ 08544

Haydn N. G. Wadley

Professor
Department of Materials Science and
Engineering,
University of Virginia,
116 Engineer's Way,
P.O. Box 499745,
Charlottesville, VA 22904

Richard B. Miles

Professor
Department of Mechanical and Aerospace
Engineering,
Princeton University,
Engineering Quad,
Olden Street,
Princeton, NJ 08544

Anthony G. Evans

Professor
Department of Mechanical Engineering,
University of California,
Engineering II,
Room 2361A,
Santa Barbara, CA 93106

A Magnetohydrodynamic Power Panel for Space Reentry Vehicles

During reentry from space, a layer of high temperature air (>3000 K) is formed extending tens of centimeters from the surface of the vehicle, well out into the high speed flow regime. Magnetohydrodynamics (MHD) can then be used to generate power by projecting magnetic fields outside the vehicle into the conducting air stream and collecting the resulting current. Here, we analyze a multifunctional MHD panel which generates the requisite magnetic fields, protects the vehicle from high temperatures, and is structurally stiff and strong. The analysis shows that a magnetic system weighing approximately 110 kg can generate 0.6 MW of power for 1000 s. [DOI: 10.1115/1.2178360]

1 Introduction

This paper explores the potential for generating large amounts of electrical power during reentry from space by exploiting magnetohydrodynamics (MHD). While the analysis below will demonstrate that there are several unresolved design issues that must be addressed before MHD generation will be usable, the authors believe that these issues are soluble given current technology. The concept envisages a vehicle whose skin is a multifunctional structure that generates magnetic fields of sufficient strength to produce useful power, while simultaneously sustaining the high heat flux, as well as the aerodynamic and structural loads, all at acceptable mass. The analysis is performed at the subelement (or panel) level. The input for design of the panel emanates from aerochemistry calculations described elsewhere [1], which are based upon a wedge-shaped vehicle configuration [2,3].

Magnetohydrodynamic power generation is described by Faraday's law. Since the ionized gas flowing over the surface of the vehicle is conductive, a magnetic field extending from the vehicle into this plasma is able to accelerate charged particles (as shown in Fig. 1) creating a transverse current density $\mathbf{J} = \sigma \mathbf{u} \times \mathbf{B}$ (neglecting, for the moment, both Hall effects and ion slip), where σ is the

conductivity of the plasma, \mathbf{u} is the velocity of the plasma, and \mathbf{B} is the local magnetic flux density. For a comprehensive discussion of power generation in a magnetohydrodynamic context, see Rosa [4].

The ensuing analysis of the usable power is based upon the following assumptions:

1. Air at $u=7$ km/s and at densities and temperatures associated with flow around a 12 deg half-angle wedge at 45 km altitude is seeded with NaK (properties as per [5]) imbuing the plasma enshrouding the vehicle with sufficient conductivity to generate ~ 1 MW of power per m^2 of surface area, provided that the magnetic field just outside the vehicle exceeds 0.2 T. This assumption is based on the aerothermodynamic model results.
2. The surface temperature of the MHD panel reaches a "steady state" of about 1500 K.
3. During the reentry period, which is assumed to last up to $t_f=1000$ s, the temperature at the magnets must remain below a maximum allowable operational limit.

The need to project a significant magnetic field beyond the surface of the vehicle encourages the use of thin walled vehicle structures that differ conceptually from the thick insulating (or ablative) tiles used in current (passive) thermal protection systems (TPS) (see, for a discussion, [6]). This paper analyzes a conceptual system comprised of a thin ceramic thermal barrier coating (TBC) strongly adhered to a metallic substrate and an active cooling system. Because of the thinness of the TBC, the interface between the insulating material and the structural alloy attains

Contributed by the Applied Mechanics Division of ASME for publication in the JOURNAL OF APPLIED MECHANICS. Manuscript received December 10, 2004; final manuscript received January 6, 2006. Review conducted by G. B. A. Younis. Discussion on the paper should be addressed to the Editor, Prof. Robert M. McMeeking, Journal of Applied Mechanics, Department of Mechanical and Environmental Engineering, University of California - Santa Barbara, Santa Barbara, CA 93106-5070, and will be accepted until four months after final publication of the paper itself in the ASME JOURNAL OF APPLIED MECHANICS.

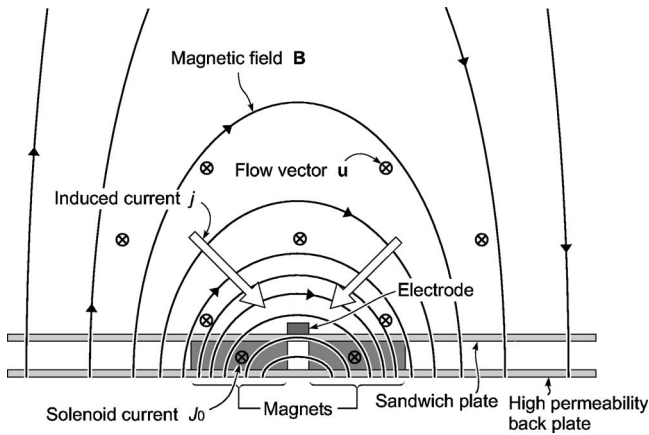


Fig. 1 Relative directions of flow, magnetic field, and generated current

high temperatures. The thermostructural consequences are analogous to those encountered in gas turbines, which use a TBC concept in conjunction with internal cooling to control the rate of thermomechanical and oxidative damage. For gas turbine applications, a robust multilayer system has been devised with two primary attributes: It satisfies thermodynamic compatibility and is tolerant to thermal and mechanical strain misfits between layers. It consists of an insulating oxide, typically yttria stabilized zirconia (YSZ), deposited as a 100–200 μm thick coating onto an aluminum-rich 20 μm thick intermetallic layer (referred to as a bond coat) that slowly oxidizes to form $\alpha\text{-Al}_2\text{O}_3$. This concept has been chosen because YSZ and $\alpha\text{-Al}_2\text{O}_3$ are thermodynamically compatible [7,8]. The bond coat is in turn deposited on a structural nickel-based superalloy, with the constraint that the interdiffusion between the alloy and the bond coat be minimal during the expected life of the system. The alloy is actively cooled by air from the intake, directed through embedded serpentine channels. While the TBC surface temperature can be as high as 1425 K in this application, the underlying materials can be as much as 200 K cooler.

A comparable TBC system is proposed for the MHD panel, but now the structural system should be nonmagnetic, lightweight, and capable of supporting loads at high temperature. These requirements, coupled with a material selection algorithm [9,10], suggest titanium alloys as a primary candidate for the vehicle skin. A bond coat concept for Ti alloys and a suitable strain-tolerant TBC oxide have yet to be devised. For the present assessment we invoke a Ti-based intermetallic bond coat that forms $\alpha\text{-Al}_2\text{O}_3$ upon oxidation, combined with a ternary oxide with lower thermal conductivity than YSZ and more resistance to sintering at the surface temperatures experienced during reentry. The candidates are, respectively, TiAl_3 and $\text{Gd}_2\text{Zr}_2\text{O}_7$ [11]. When deposited as a columnar structure using electron beams, $\text{Gd}_2\text{Zr}_2\text{O}_7$ has a thermal conductivity, $k=0.5$ W/mK [11], but this conductivity can potentially be lowered [12] by manipulating the morphology of the porosity, possibly by as much as a factor of two [13,14].

The TBC would be deposited onto a multifunctional panel that performs four functions: (a) impedes heat transfer into the vehicle; (b) supports an integral cooling system; (c) contains embedded magnets; and (d) withstands large compressive and bending loads. A truss core sandwich design made using a Ti alloy is proposed. When optimized for load capacity, the weight of such panels as a function of the load is summarized in Fig. 2, relative to a solid panel of the same mass per unit area [15,16]. The open channels in the core allow cooling and permit permanent or solenoid magnets to be incorporated, as elaborated later.

This study explores the feasibility of using such a design to

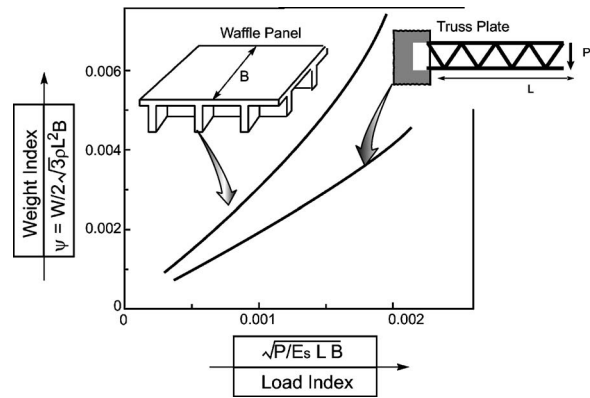


Fig. 2 Mass of truss-core panels as a function of load capacity, compared to solid beams

generate power during reentry, and will propose a systematic means for design and optimization. The analysis reveals that a MHD panel competes effectively with other power sources in terms of power density and energy density (see Fig. 3).

The paper is organized in the following manner. (a) The design concept is outlined. (b) The power that can be generated is related to magnetic field strength and the flow conditions. (c) Magnetic field strengths are calculated using finite elements. (d) The optimization approach is described. (e) The panels are optimized and trends in net power generated are established. The trends are used to provide a focus for future research that addresses feasibility and validation of the models.

2 Design Concept

The panel concept, illustrated in Fig. 4, embeds either resistive solenoid magnets (shown here) or permanent magnets (not displayed). (Superconducting magnets are discounted at this stage due to unresolved cooling requirements.) The basic panel design is a 50 mm thick titanium sandwich panel, comprising two 5 mm thick faces and a 40 mm thick truss core. The reentry maneuvers determine the maximum structural loads; these are mission-dependent and are not explicitly analyzed. Based on previous assessments of the strength and stiffness of truss core panels [15,17], it is believed that the proposed panel can be designed to sustain the required loads at acceptable weight. Because the core of the panel contains open channels, and because the truss struc-

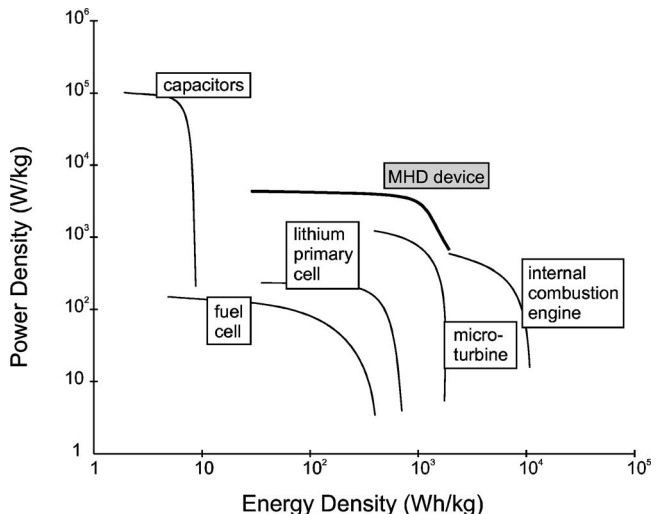


Fig. 3 Ragone plot for various power sources for a reentry vehicle including the proposed MHD device

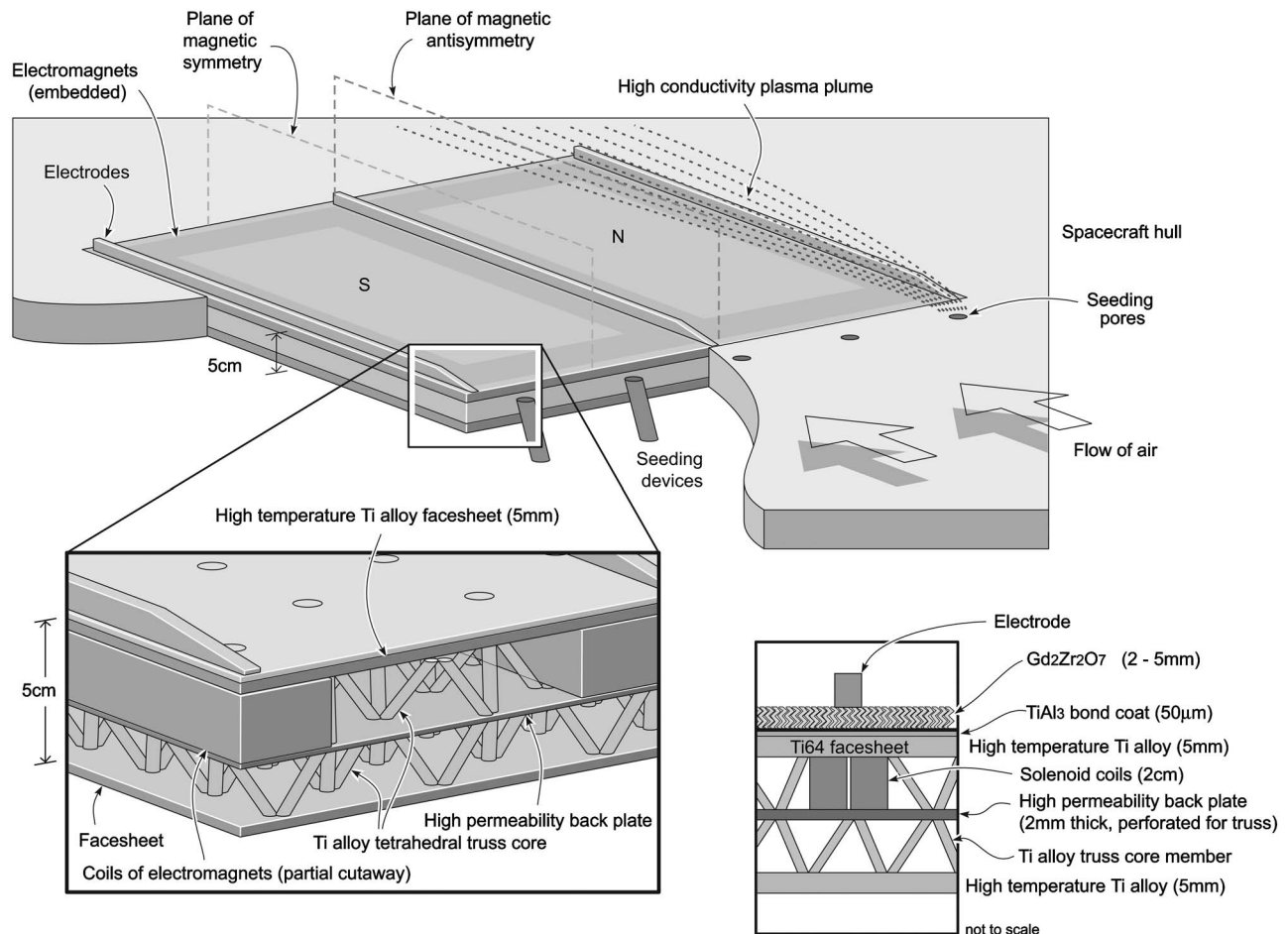


Fig. 4 Array of rectangular solenoids contained in a multifunctional truss-core sandwich structure

tures efficiently conduct heat from the faces, this panel enables simultaneous thermal management by active cooling. The magnetic array is relatively long in the direction of the flow stream, whereupon edge effects at the front and back can be neglected. The array is periodic in the width direction, which increases the magnetic field strengths [18,19]. To realize this potential, adjacent magnets must be oriented with alternating north and south poles, creating flux loops. By placing electrodes at the junctions between the magnets, the current is directed to these electrodes and collected, thereby generating power, as sketched in Fig. 1. Moreover, the symmetry simplifies the calculations required. The magnetic array is separated from the surface of the vehicle by a titanium alloy face and a TBC layer.

For the resistive solenoid design in Fig. 4, the north and south poles of the magnetic elements alternate. This particular array contains two periodic elements. Electrodes for power collection are mounted on the surface of the TBC, interlaced between the magnet poles. The design variables are the thickness h and total width $2w$ of the solenoid, the width of the arms of a single solenoid b , and the current density in the solenoid J_0 . Again, it is assumed that the length L of the array is much larger than any other geometric variable, permitting a two-dimensional approximation. Additional variables, such as the geometry of the high-permeability backing plate, will not be addressed. The overall configuration of a permanent magnet array is similar. Comparable fields can be achieved with a variety of alternative configurations.

Thin layers of insulation are used in conjunction with active cooling of the sandwich face. The titanium alloy face layer beneath the TBC uses an embedded planar heat pipe to assure adequate creep strength by preventing the temperature from exceed-

ing 900 K. Active cooling protects the upper surfaces of the magnets, preventing them from exceeding 500 K, their maximum operational temperature. This design uses water, which is heated from 273 K to 373 K, evaporated, and expelled from the vehicle. There are several precedents for a cooling system of this type, including Faghri [20]. In such a system, each kilogram of water would expel 2.8 MJ of heat from the vehicle. The mass of the cooling system, m_{cool} is considered to be that of the water m_w , plus a re-circulation system ϵm_w such that $m_{cool} = (1 + \epsilon)m_w$. Active cooling is required to dissipate the heat associated with the operation of resistive solenoids.

3 Estimation of Power Generated

The power P_0 delivered to the load, per unit volume of flow over the vehicle, is

$$P_0 = K(1 - K)\bar{\sigma}u^2B^2 \quad (1)$$

where K is the load factor which is between zero and one, $\bar{\sigma}$ is an effective conductivity of the gas which accounts for Hall effects, u is the magnitude of the velocity of the flow stream, and B is the norm of magnetic flux density; $B = \|\mathbf{B}\|$. The velocity \mathbf{u} is perpendicular to the magnetic field \mathbf{B} . The maximum power that can be extracted from the flow occurs when the load impedance equals the resistance of the current passing through the air, and $K=0.5$. The use of Eq. (1), which is derived for a one-dimensional magnetic field, can be justified because, for the magnetic fields examined here, at all locations the vector product of the fluid velocity and the magnetic field is directed toward the electrodes. Ion slip effects have been shown to be negligible at 46 km altitude by

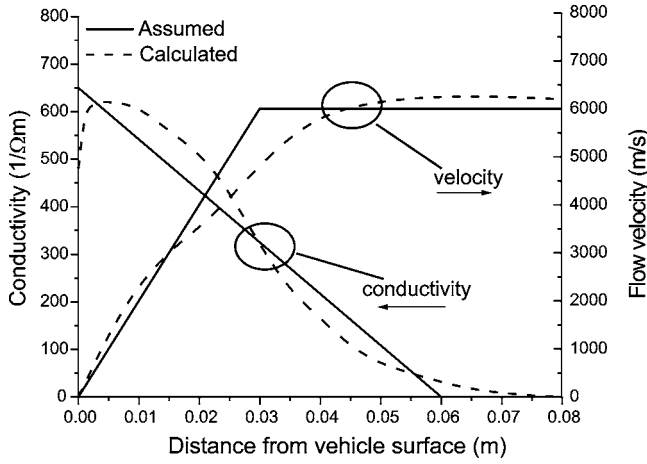


Fig. 5 Comparison of assumed and calculated conductivity and velocity profiles with distance from vehicle surface

Macheret et al. [1]. The remaining elements of Eq. (1) are addressed below.

3.1 Plasma Conductivity. The conductivity is a function of the density and composition of the flow stream, the configuration of the shock system, the gas temperature, and the presence or absence of artificial seeding. We assume that the conductivity arises principally because of artificial seeding, and that the seeding device projects the seed 0.06 m from the vehicle surface. Calculation of conductivities requires a multispecies nonequilibrium flow model, which is beyond the scope of this paper but has been performed by [1]. The seeding model used by [1] assumed 1% by mass NaK entrained in the flow ahead of the MHD region; during a 1000 s flight, this would require only 1–2 kg of seed plus some additional mass for an injection system which would be similar to fuel injection systems for ramjet engines. Because our purpose is to compare magnetic arrays, we simplify by regarding the conductivity as varying linearly within the region of interest

$$\sigma(z) = \sigma_0[(z_0 - z)/z_0], \quad (2)$$

where $\sigma_0 = 650/\Omega\text{m}$ and $z_0 = 0.06$ m. This is consistent with gas properties at an altitude of approximately 45 km, and reflects the distribution of temperature and seed material through the boundary layer in the calculations by Macheret et al. [1]. A comparison of the assumed distribution of conductivity with the distribution calculated by Macheret et al. [1] is shown in Fig. 5.

At high magnetic fields and low collision frequencies, the electrons circulate around the magnetic field lines rather than migrate between the electrodes leading to a Hall current and a significant reduction of the effective conductivity. If the Hall parameter Ω_e (the ratio of the cyclotron frequency of the electrons to the collision frequency) is greater than one, the Hall effect must be taken into account. In this case, the effective conductivity $\tilde{\sigma}$ is written

$$\tilde{\sigma} = \frac{\sigma}{1 + \Omega_e^2} = \frac{\sigma}{1 + (\mu_e B)^2} \quad (3)$$

where μ_e is the electron mobility (with $\mu_e B$ an alternate representation of the Hall parameter). Assuming an electron mobility $\mu_e = 10/T$, the Hall parameter is unity when flux density $B = 0.1$ T. Operation at magnetic field strengths much above 0.2 T does not lead to a significant increase in power extraction without the introduction of complex electrode segmentation and the potential of interelectrode voltage breakdown. In this analysis it is assumed that continuous Faraday electrodes are used. It should also be noted that 0.2 T is close to the limit of the magnetic field strength that can be generated from reasonable steady state electromagnet configurations.

3.2 Flow Velocity. Various assumptions need to be made about the flow over the vehicle.

1. The velocity increases linearly with distance z from the vehicle surface, starting at zero and reaching the velocity in the shock layer u_0 at the edge of the boundary layer. Outside the boundary layer, the velocity is constant and equal to the shock layer velocity.
2. The thickness of the boundary layer, $t_{BL} = 0.03$ m [1].
3. The magnetic Reynolds number is small, and hence the flow does not significantly perturb the magnetic field.

The resulting velocity function is

$$u(z) = \begin{cases} u_0 \left(\frac{z}{t_{BL}} \right) & \text{if } z \leq t_{BL} \\ u_0 & \text{if } z > t_{BL} \end{cases} \quad (4)$$

This velocity function is compared with detailed aerothermodynamic calculations [22] in Fig. 5.

The power generated by the MHD device, per unit volume, thus becomes

$$P_0 = \frac{\sigma(z)u(z)^2 B^2}{4[1 + (10B)^2]}, \quad (5)$$

where $u(z)$ is given by Eq. (4), $\sigma(z)$ is given by Eq. (2), and the magnetic flux density B is determined as detailed below. This function is integrated over the width of a magnetic element and the thickness of the conductive layer in order to determine the power generated, per unit length, by a single periodic magnetic element.

4 Magnetic Field Calculations

Finite element calculations performed with FEMLAB [23] have been used to develop a relationship for the dependence of power generation on the geometry and composition of the magnetic array. These computations provide the relationship between geometric variables (thickness h , element width $2w$, and solenoid arm width b), internal variables (current density J_0 or magnetization M_0), and the magnetic fields. The finite element results generate a database of magnetic fields as a substitute for an explicit functional relationship between the power generated and the geometric and array parameters.

An example is provided for the electromagnetic arrays. Because of the magnetic symmetries and antisymmetries and the assumption of periodicity, as shown in Fig. 4, only half of one periodic element needs to be modeled. Consider a magnetic field, intensity \mathbf{H} , and a boundary with normal $\hat{\mathbf{n}}$. Along a plane of magnetic symmetry, the condition $\hat{\mathbf{n}} \cdot \mathbf{H} = 0$ holds; (magnetic field lines do not cross the boundary). Similarly, on a plane of magnetic antisymmetry, the boundary condition is $\hat{\mathbf{n}} \times \mathbf{H} = 0$ (magnetic field lines crossing the boundary have no component parallel to the boundary). The magnetic flux density is given by $\mathbf{B} = \mu \mathbf{H}$, where μ is the permeability of the medium.

A typical result is presented in Fig. 6 for a solenoid of thickness $h = 0.02$ m, arm width $b = 0.12$ m, solenoid half-width $w = 0.3$ m, with current density $J_0 = 15$ MA/m². The backing plate is assumed to be 0.01 m thick with relative permeability $\mu_r = 20,000$. It would be more realistic to use a thinner, more highly permeable back plate, but this choice would diminish the computational efficiency. The titanium face sheet and TBC layer have relative permeability near unity, and are not modeled explicitly. The plane $x = 0$ m exhibits magnetic symmetry, while the plane $x = 0.3$ m is a plane of magnetic antisymmetry. The region from which power can be extracted is marked "region of high conductivity".

For each such FEMLAB calculation, the expression (5) is integrated over the region of high conductivity, and the total power generated per periodic tile is twice the value of this integral (since only half of one periodic element is modeled). This power gen-

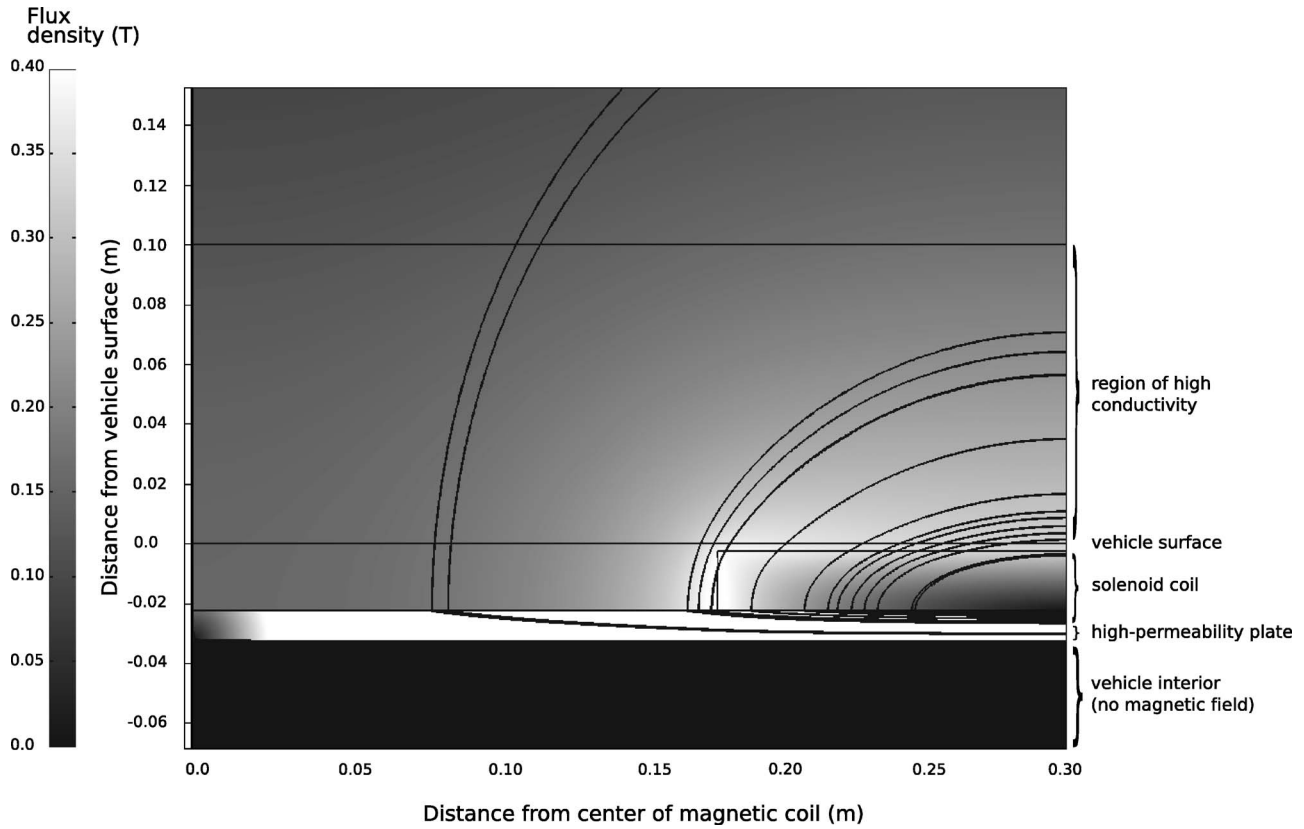


Fig. 6 Typical FEMLAB calculated result showing magnetic flux density (T) (with bar to the left) and a representative set of magnetic field lines. This configuration is for a solenoid with current density $J_0=15 \text{ MA/m}^2$, of thickness $h=0.02 \text{ m}$, arm width $b=0.12 \text{ m}$, and solenoid half-width $w=0.3 \text{ m}$. Note that the magnetic flux density in the back plate is very high, while the magnetic flux density in the vehicle is negligible.

eration is an input to the optimization procedure. Further finite element calculations suggest that the power generation capacity for a tile at the edge of a periodic array is reduced by approximately 15%. Thus, an array of N periodic tiles will produce power per meter length equal to

$$P_{\text{tot}} = (N - 0.3)P \quad (6)$$

where P refers to the integral of P_0 (Eq. (5)) over the width of the magnetic element and the thickness of the conductive layer.

5 Optimization Scheme

5.1 Power/Mass Exchange Constant. To optimize the configuration of the magnetic array, we define the effective power \hat{P} which becomes the objective function

$$\hat{P} \equiv P_{\text{net}} - \gamma m_{\text{tot}} \quad (7)$$

In this formula, P_{net} is the net power generated by the panel (the total power generated less the power required to run the magnets) and m_{tot} is the total mass of the magnets plus the cooling system. The power/mass exchange constant γ is interpreted as the penalty associated with each unit of mass of the MHD device. Accordingly, the effective power \hat{P} is the difference between the net power generated and the total penalty associated with the mass of the device. For specified γ , the optimal design is that maximizing the effective power \hat{P} .

If γ is progressively varied, a locus of optimal designs in $(m_{\text{tot}}, P_{\text{net}})$ space arises, as shown in Fig. 7. Note that a minimum mass of magnets m_{min} is required before any power can be generated. Graphically, the net power density (the ratio of net power to total mass) is maximized at the point where a ray from the

origin is tangent to the locus, which implies that the slope of the locus must be equal to the net power density. At every point on the locus, since \hat{P} is a maximum

$$\delta \hat{P} = \delta P_{\text{net}} - \gamma \delta m_{\text{tot}} = 0 \quad (8)$$

such that γ is the slope of the locus. Hence we must find the point where the net power density is equal to γ . When $\hat{P}=0$

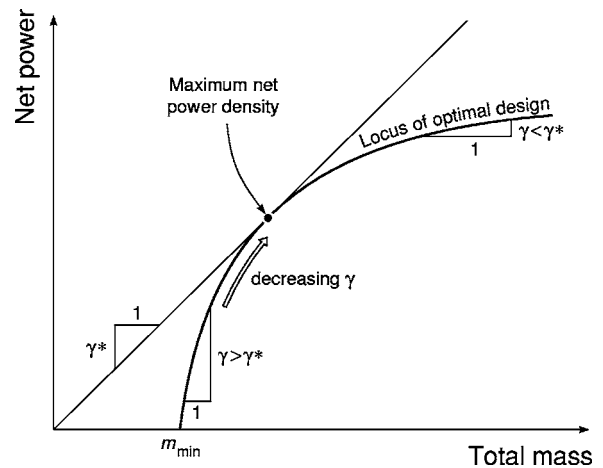


Fig. 7 The locus of optimal designs in $(m_{\text{tot}}, P_{\text{net}})$ space, showing the construct to obtain the maximum net power density. The maximum net power density is found when a ray from the origin is tangent to the locus.

$$\gamma|_{\dot{P}=0} = \frac{P_{\text{net}}}{m_{\text{tot}}} = \gamma^* \quad (9)$$

Thus γ can also be interpreted as the maximum net power density by finding the value of $\gamma = \gamma^*$ for which the maximum of $\dot{P}=0$.

5.2 The Optimization. Optimization involves an exchange between total mass (the MHD device plus the coolant) and power generation, dependent upon flight time t_f and heat flux q . Because the mass of the structural elements and insulation will be present whether or not a MHD device is incorporated, this mass need not be considered for optimization. To determine the number of periodic elements N (noting that fractional elements are not permissible), the maximum width of the array is taken to be 1.2 m. The power surplus P_{net} (per unit length) is the power generated P_{tot} less the power expended by the magnetic array P_{exp} . For permanent magnets $P_{\text{exp}}=0$, while for a resistive solenoid system

$$P_{\text{exp}} = 2N \frac{J_0^2 h b}{\sigma_s} \quad (10)$$

where σ_s is the conductivity of the solenoid material (at 373 K, the expected operating temperature of the solenoids, for copper $\sigma_s=4.6 \times 10^7/\Omega\text{m}$, while for aluminum, $\sigma_s=2.8 \times 10^7/\Omega\text{m}$). A resistive electromagnet generates heat equal to the power required to run the solenoid P_{exp} .

The mass of the solenoid array (per unit length) is

$$m_{\text{mag}} = 2Nbh\rho \quad (11)$$

where ρ is the density of the material used in the array (for copper, $\rho=8960 \text{ kg/m}^3$, and for aluminum, $\rho=2702 \text{ kg/m}^3$), and the mass of a neodymium-iron-boron permanent magnet array is

$$m_{\text{mag}} = 2Nwh\rho \quad (12)$$

with $\rho=7500 \text{ kg/m}^3$.

The steady-state flow of heat through the TBC is dictated by its thermal conductivity k , the difference in temperature between the two sides ΔT , and its thickness t_{TBC}

$$H_{\text{surf}} = 2Nw \frac{k\Delta T}{t_{\text{TBC}}} \quad (13)$$

where $2Nw$ is the total width of the panel. Transients are considered to be of short duration. The temperature difference is considered to be governed by the temperature attained on the external surface of the TBC (1500 K), ascertained by the aerothermodynamic calculations,¹ and the maximum temperature that a titanium alloy can sustain to assure adequate creep strength (900 K). The total heating input is

$$H_{\text{tot}} = H_{\text{surf}} + P_{\text{exp}} \quad (14)$$

The mass of the cooling system is

$$m_{\text{cool}} = (1 + \epsilon) \frac{H_{\text{tot}} t_f}{C_{\text{water}}} \quad (15)$$

where C_{water} is the energy per unit mass to heat and evaporate the water. It is assumed that the water vapor is immediately vented from the vehicle through an insulated system, such that no further heating of the vehicle occurs. The total mass of the system is thus $m_{\text{tot}}=m_{\text{mag}}+m_{\text{cool}}$, and the effective power generation can be evaluated for each candidate design. Note that the quantities calculated here are per unit length of the MHD panel.

¹Calculations by Candler [22] indicate that the total heating rate on the vehicle surface is approximately in equilibrium with radiative cooling and heat flux into the vehicle when the surface temperature is 1500 K.

Table 1 Standard values for optimization parameters

Parameter	Value
Exchange constant γ	5 kW/kg
Flight time t_f	1000 s
TBC thermal conductivity k	0.5 W/mK
Temperature gradient through TBC ΔT	600 K
Cooling system mass coefficient ϵ	0.15
Total panel width w_{tot}	1.2 m
Shock layer velocity u_0	6 km/s
Plasma conductivity σ_0	100/ Ωm
Reference TBC thickness	2.5 mm
Potassium seeding (by mass)	1%

6 Optimization Results

The initial optimization will be performed using the parameters in Table 1. Thereafter the separate influences of several parameters will be explored.

A wide search through probable candidates for geometric and internal variables (including all combinations of those in Table 2) indicates that an optimal design is achieved by using an aluminum solenoid with element width $2w=0.6 \text{ m}$, solenoid arm width $b=0.12 \text{ m}$, solenoid thickness $h=0.02 \text{ m}$, TBC thickness $t_{\text{TBC}}=0.0025 \text{ m}$, and current density $J_0=12 \text{ MA/m}^2$ (equivalent to 28,800 amp turns). This array generates a net power $P_{\text{net}}=538 \text{ kW/m}$. The total power generated is 588 kW/m, with 50 kW/m expended to power the solenoid. The mass of the solenoid is 26 kg/m, and the mass of coolant is 79 kg/m. At very long flight times, $t_f > 6000 \text{ s}$, copper becomes preferable to aluminum because of its higher conductivity. Permanent magnetic arrays are uniformly rejected because the magnetic fields are not sufficiently large to be competitive.

The procedure is illustrated by results for the net power/total mass at fixed TBC thickness (Fig. 8) with each curve representing a specific thermal conductivity. Each point on every curve represents a design with maximum effective power. Note that the shapes of the curves are similar to that shown in Fig. 7.

Variations of net power density with power are illustrated in Fig. 9. This plot shows that power density can be significantly increased by increasing the thickness of the TBC. It is also apparent that there is a maximum net power density for each value of TBC thickness.

Trends in the maximum are reexpressed in Fig. 10, using the loci through the maxima of each curve in Fig. 9. This result provides direct guidelines for the material to be used as the thermal barrier (based on the thermal conductivity range) and the thickness required to achieve the maximum net power density. It is

Table 2 Values of design parameters used in the finite element simulations. Note that the values used for the solenoid arm width b are dependent upon the solenoid half-width w ; b is taken to be the integral part of the calculation.

Design parameter	Values simulated
Solenoid half-width w (m)	0.1, 0.12, 0.15, 0.20, 0.25, 0.30, 0.60
Solenoid thickness h (m)	0.01, 0.015, 0.02, 0.0225, 0.025, 0.03, 0.04, 0.045
Solenoid arm width b (m)	$w/7 \times (1, 1.5, 2, 2.5, 3, 3.5, 4, 4.5, 5, 6)$
Thickness of TBC layer t_{TBC} (mm)	1, 1.5, 2, 2.25, 2.5, 2.75, 3, 3.5, 4, 4.5, 5
Current density J_0 (MA/m ²)	10, 11.25, 12, 13.25, 14.25, 15, 15.5, 16.25, 17.5, 20, 22.5, 25, 30, 35, 40

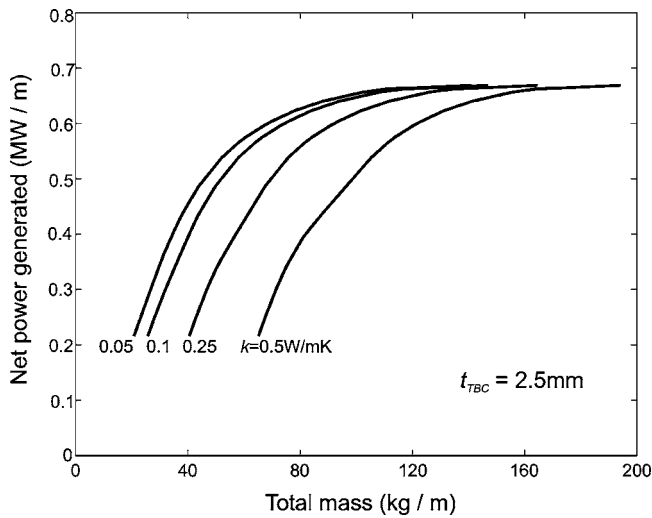


Fig. 8 Net power generation versus total mass at constant TBC thickness $t_{TBC}=2.5$ mm for varying TBC thermal conductivity

clear that maximum net power density increases rapidly as k is decreased below 0.2 W/mK; when k is very low, the TBC thickness becomes less important.

Varying the number of magnetic elements reveals that the maximum effective power occurs when $N=2$. This optimum arises because the increase in the flux density near the surface of the vehicle upon increasing N is counteracted by the rate at which the flux density declines with distance from the vehicle. The enhancement in net power enabled by reducing the extra weight of the cooling system is indicated on Fig. 11. At low γ , the design is not sensitive to the cooling system efficiency, because the additional mass of cooling water does not carry a large weight penalty. As γ increases, the design becomes more sensitive to cooling system efficiency. This figure expresses the benefit of designing a lightweight pumping system.

7 Implications

The analysis has demonstrated that MHD power panels located within a re-entry vehicle have the potential to generate usable

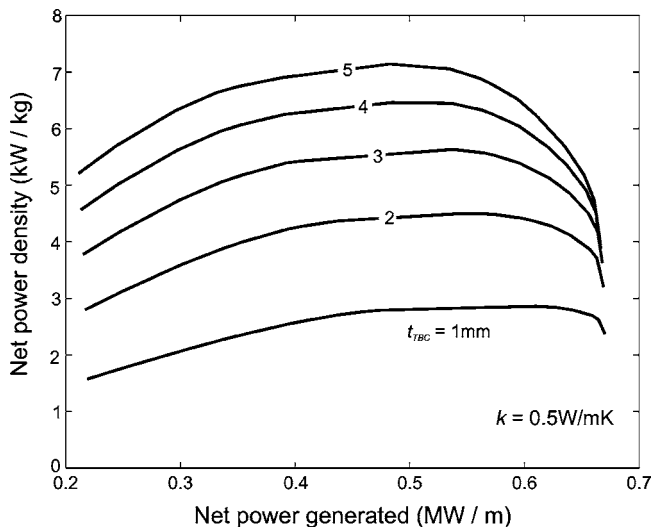


Fig. 9 Net power density as a function of net power for constant TBC thermal conductivity $k=0.5$ W/mK and varying TBC thickness

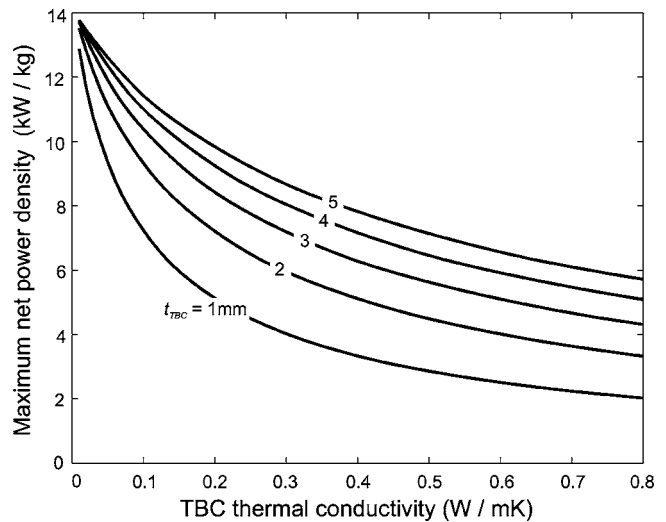


Fig. 10 Maximum net power density as a function of TBC thermal conductivity for varying TBC thickness

power. The optimization indicates that it is possible to design a 1.2 m wide panel which will generate 0.6 MW/m length at a total mass of approximately 110 kg/m. However, stringent technological challenges need to be satisfied before such a panel can be brought to fruition.

1. Effective injection and mixing of the seed material are essential and remain to be demonstrated.
2. Water must be stored on board and a lightweight recirculation system developed that pumps the water through the panel and then ejects it from the vehicle.
3. A thermal barrier material with low thermal conductivity, such as $Gd_2Zr_2O_7$, must be deposited on the surface of the panel at unprecedented thickness. It must resist spalling during manufacturing, as well as when subject to a thermal gradient on reentry.
4. A bond coat must be developed for titanium alloys that survives manufacturing and remains intact when exposed to reentry.

The importance of thermal management is emphasized: For the example cases, approximately 75% of the total mass of the MHD

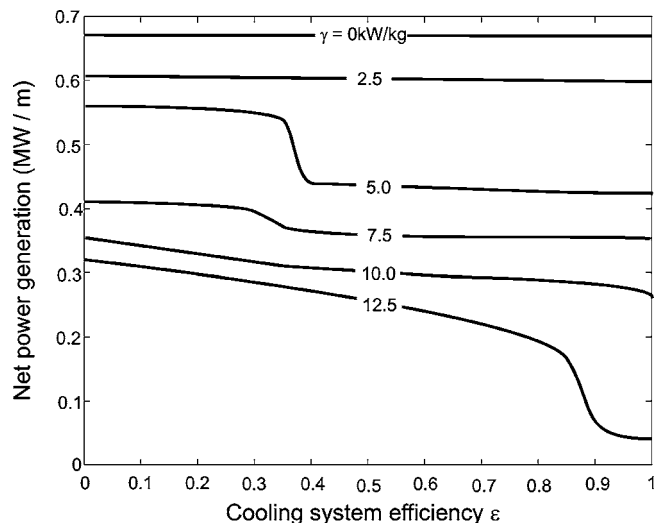


Fig. 11 Variation of net power generation with the cooling system mass coefficient ϵ

system is coolant. Preliminary materials and manufacturing assessments indicate that $Gd_2Zr_2O_7$ having the requisite thickness can be deposited onto superalloys by using plasma-assisted, directed vapor deposition (DVD) [24]. It remains to determine whether $Gd_2Zr_2O_7$ can be deposited on titanium alloys at the required thickness and pore structure and adhere, as well as resist delamination in a thermal gradient. Depositing a bond coat on the alloy that oxidizes to form $\alpha-Al_2O_3$, such as $TiAl_3$, would be essential. These materials and manufacturing issues would need to be clearly specified and resolved before embarking on MHD panel development.

Acknowledgment

The authors are grateful for financial support from DARPA—Defense Science Office, and for extensive discussions with and numerical modeling by Prof. Graham Candler at the University of Minnesota, and Dr. Mikhail Shneider and Dr. Sergej Macheret at Princeton University.

References

- [1] Macheret, S. O., Shneider, M. N., and Candler, G. V., 2004, "Modelling of MHD Power Generation on Board Reentry Vehicles," Paper No. AIAA-2004-1024.
- [2] Hankey, W. L., and Elliot, G. A., 1968, "Hypersonic Lifting Body Optimization," *J. Spacecr. Rockets*, **5**(12), pp. 1463–1467.
- [3] Kolodziej, P., Bowles, J. V., and Roberts, C., 1998, "Optimizing Hypersonic Sharp Body Concepts from a Thermal Protection System Perspective," 8th, AIAA Paper No. 98-1610.
- [4] Rosa, R. J., 1968, *Magnetohydrodynamic Energy Conversion*, McGraw-Hill, New York.
- [5] Callery Chemical Company, 2002, "Potassium-Sodium Alloy (NaK)," Product data sheet.
- [6] Woods, B., 2003, "Heated Debates: A History of the Development of the Space Shuttle's Thermal Protection System: 1970-1981," *Quest*, **10**(3), pp. 39–55.
- [7] Miller, R. A., 1984, "Oxidation-Based Model for Thermal Barrier Coating Life," *J. Am. Ceram. Soc.*, **67**, pp. 517–521.
- [8] Evans, A. G., Mumm, D. R., Hutchinson, J. W., Meier, G. H., and Pettit, F. S., 2001, "Mechanisms Controlling the Durability of Thermal Barrier Coatings," *Prog. Mater. Sci.*, **46**, pp. 505–553.
- [9] Ashby, M. F., 1989, "Materials Selection in Conceptual Design," *Mater. Sci. Technol.*, **5**(6), pp. 517–525.
- [10] Ashby, M. F., 1999, *Material Selection in Mechanical Design*, 2nd ed., Butterworth-Heinemann, Oxford, UK.
- [11] Maloney, M. J., 2001, "Thermal Barrier Coating Systems and Materials," U.S. Patent 6,177,200, United Technologies Corporation, Hartford, CT.
- [12] Nicholls, J. R., Lawson, K. J., Johnstone, A., and Rickerby, D. S., 2002, "Methods to Reduce the Thermal Conductivity of eb-pvd tbc's," *Surf. Coat. Technol.*, **151–152**, pp. 383–391.
- [13] Lu, T. J., Levi, C. G., Wadley, H. N. G., and Evans, A. G., 2001, "Distributed Porosity as a Control Parameter for Oxide Thermal Barriers Made by Physical Vapor Deposition," *J. Am. Ceram. Soc.*, **84**(12), pp. 2937–2946.
- [14] Hass, D. D., Slifka, A. J., and Wadley, H. N. G., 2001, "Low Thermal Conductivity Vapor Deposited Zirconia Microstructures," *Acta Mater.*, **49**(6), pp. 973–983.
- [15] Wicks, N., and Hutchinson, J. W., 2001, "Optimal Truss Plates," *Int. J. Solids Struct.*, **38**(30–31), pp. 5165–5183.
- [16] Evans, A. G., 2001, "Lightweight Materials and Structures," *Mater. Res. Soc. Bull.*, **26**(10), pp. 790–797.
- [17] Chiras, S., Mumm, D. R., Evans, A. G., Wicks, N., Hutchinson, J. W., Dharmasena, H. N., Wadley, H. N. G., and Fichter, S., 2002, "The Structural Performance of Near-optimized Truss Core Panels," *Int. J. Solids Struct.*, **39**(15), pp. 4093–4115.
- [18] Kovalev, K. I., and Markina, T. A., 1995, "Power Facility with a Built-in Multipole MHD Generator," *High Temp.*, **33**, pp. 463–472.
- [19] Bityurin, V. A., Bocharov, A. N., and Lineberry, J. T., 1999, "MHD Aerospace Applications," *13th International Conference on MHD Power Generation and High Temperature Technologies*, Vol. III, Beijing, Oct. 12–15, IEE CAS, Beijing, pp. 793–814.
- [20] Faghri, A., 1995, *Heat Pipe Science and Technology*, Taylor & Francis, London.
- [21] Sudmeijer, K. J., Buursink, J., and Lopes, C., 2003, "A Low-cost Active Cooling Mechanism to be Used on Future Launchers," *Space Technol.*, **23**(2–3), pp. 87–103.
- [22] Candler, G., 2003, Private communication.
- [23] FEMLAB, 2003, Comsol Inc., Burlington MA.
- [24] Hass, D. D., Groves, J. F., and Wadley, H. N. G., 2001, "Reactive Vapor Deposition of Metal Oxide Coatings," *Surf. Coat. Technol.*, **146**, pp. 85–93.